Received 9 November 2021; revised 27 December 2021; accepted 5 January 2022. Date of publication 20 January 2022; date of current version 7 October 2022.
The review of this article was arranged by Editor J. Tang.

Digital Object Identifier 10.1109/JEDS.2022.3142769

Low-Temperature Solution-Processed All Organic Integration for Large-Area and Flexible High-Resolution Imaging

XIAO HOU[1], SUJIE CHEN[1] (Member, IEEE), WEI TANG[1] (Member, IEEE), JIANGHU LIANG[2], BANG OUYANG[1] (Graduate Student Member, IEEE), MING LI[1], YAWEN SONG[1] (Graduate Student Member, IEEE), TONG SHAN[1], CHUN-CHAO CHEN[2], PATRICK TOO[3], XIAOQING WEI[4], LIBO JIN[4], GANG QI[5], AND XIAOJUN GUO[1] (Senior Member, IEEE)

1 School of Electronic Information and Electrical Engineering, Shanghai Jiao Tong University, Shanghai 200240, China
2 School of Materials Science and Engineering, Shanghai Jiao Tong University, Shanghai 200240, China
3 FlexEnable, Cambridge CB4 0FX, U.K.
4 iRay Technology, Shanghai 215000, China
5 Tianma Microelectronics, Shanghai 201201, China

CORRESPONDING AUTHOR: X. GUO (e-mail: x.guo@sjtu.edu.cn)

This work was supported in part by the National Key Research and Development Program of China under Grant 2019YFA070610; in part by the National Science Fund for Excellent Young Scholars under Grant 61922057; and in part by the Shanghai-U.K. Industrial Challenge Programme under Grant 104009.

ABSTRACT A facile blade-coating process is developed for large area deposition of uniform thick organic active layers in organic photodiodes (OPDs). Large-area semi-transparent top metal electrodes are thermally evaporated with an optimal deposition rate to achieve good balance between transparency and conductivity for top illumination integration structure with the organic thin-film transistor (OTFT) backplane. The maximum process temperature of the OPD is 85 °C, so that the performance of the OTFT underneath is not affected. Based on the developed integration structure and processes, an all-organic integrated flexible active-matrix imager is developed, having the largest size (130 mm × 130 mm), highest resolution (1536 × 1536 pixels, 300 ppi) and lowest process temperature (100 °C) reported so far for the OPD based imagers.

INDEX TERMS Organic photodiode, organic thin film transistor, large area, active-matrix imager, flexible electronics.

I. INTRODUCTION

With advances of silicon photodiodes and technology scaling of the complementary metal-oxide-semiconductor (CMOS) technology, the CMOS image sensor (CIS) has experienced explosive growth over the past decade in applications for mobile imaging, digital cameras, optical sensors, biomedical inspection and industrial machine vision [1]–[10]. However, many application scenarios are not able to be addressed by the CIS technology, especially when large-area coverage and free form factor (e.g., being flexible or conformable) is required [11]–[13]. The typical examples include x-ray imagers [14]–[17], scanners [18], in-display full or half screen fingerprint recognition [19], interactive flat-panel displays and emerging bio-inspired visual systems [20]–[23].

To meet these application requirements, active matrix addressed imaging arrays are implemented by integrating the photodiodes with the thin-film transistor (TFT) pixel switches in large area fabrication processes [24]–[26]. A combination of the hydrogenated amorphous silicon (a-Si:H) TFT and the a-Si:H photodiode has become the most well-developed technology solution for manufacturing commercial high-resolution imagers [26]. The amorphous indium-gallium-zinc-oxide (IGZO) TFT also attracts interests for active-matrix imagers attributed to its higher mobility and lower leakage current, but its performance

is very sensitive to the hydrogen-rich a-Si:H photodiode processes, causing integration challenges [27], [28]. Although the low temperature polysilicon (LTPS) TFT is able to be used to build high-resolution sensor array with in-pixel signal amplification, it suffers large leakage current and high manufacturing cost [10].

Compared to the a-Si:H photodiode, the organic photodiode (OPD) owns advantages of wide range tunable photoelectrical properties, and low-temperature facile processes very friendly to the TFT backplanes [16], [29]–[31]. There have been lots of work on OPD based active-matrix imaging arrays, which used inorganic TFT backplanes including a-Si:H, a-IGZO and LTPS [32]–[33]. In short term, it is good choice to leverage the industry available processes for mass manufacturing. However, in long term, it would be a more ideal route to integrate the OPD with the organic TFT (OTFT) backplane, and thus fully exploit the advantages of organic electronics. With the rapid development of soluble organic semiconductors and their matched material stacks, the OTFT can achieve better performance figure of merits in mobility, leakage current and stability than those of the a-Si:H TFT [34]–[36]. With such all organic integration, low processing temperature and well-matching of both thermal and mechanical properties with the common plastic films are able to achieved for building ubiquitous imagers of highly customizable form factors. Attributed to these potential advantages, there have been work on active-matrix imager arrays integrating OPDs and OTFTs, but of relatively small size and low resolution [37]–[39].

In this work, a facile large-area blade-coating process is developed for large area deposition of uniform thick organic active layers in OPDs. Large-area semi-transparent top metal electrodes are thermally evaporated with an optimal deposition rate to achieve good balance between transparency and conductivity for top illumination structure. The maximum process temperature of the OPD is 85 °C, so that the performance of the OTFT underneath is not affected. Based on the developed OTFT-OPD integration structure and processes, a 130 mm × 130 mm size flexible active-matrix imager with 1536 × 1536 pixels (about 300 ppi) and a pixel size of 85 μm × 85 μm is developed.

II. EXPERIMENTAL METHODS

The pixel circuit used for the active-matrix imager is illustrated in Fig. 1(a) composed of an OPD for photo sensing and an OTFT as the switch. To realize such all organic integration, an inverted structure bulk heterojunction (BHJ) OPD was vertically stacked on top of the OTFT backplane (Fig. 1(b)). The OTFT backplane was fabricated with a top-gate bottom-contact (TGBC) structure on polyethylene naphthalate (PEN) substrate [40]. With the bottom-contact structure, the source/drain electrodes were deposited before the OSC layer, so that the mature metallization techniques with sputtering and photolithography were conveniently used for micrometer-resolution electrode patterns.

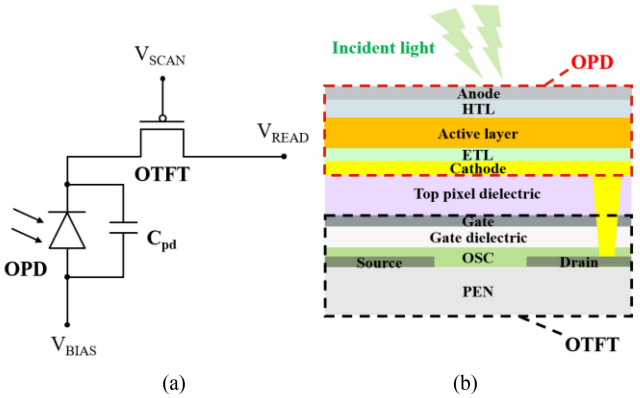

FIGURE 1. (a) Pixel circuit for the active matrix imager, consisting of a switch OTFT and an OPD. (b) Schematic of the cross-sectional OPD-OTFT integration structure.

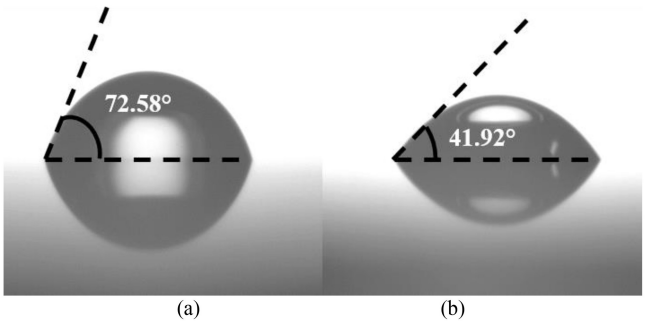

FIGURE 2. The measured deionized water contact angle of the Au pixel electrode surface (a) before and (b) after O_2 plasma treatment for 5 minutes.

Compared to the bottom-gate bottom-contact structure, the TGBC one owns larger carrier injection area for smaller contact resistance [41]–[43]. When being used in photo imagers, the top gate metal can also shield the light from the top. A full material stack, including the OSC layer, the polymer dielectric layer and the interfacial layer, was developed for the TGBC structure to achieve reliable and uniform performance with large area solution coating processes at low temperature less than 100 °C [44]. After completing the intrinsic OTFT part, a polymer dielectric passivation layer was deposited by solution coating. The top Au pixel electrode layer was connected to the metal layer underneath through via interconnections formed by dry etching. Before the OPD processes, the Au electrode surface was treated by oxygen plasma of power 29.6 W for 5 minutes to become less de-wetting (Fig. 2).

ZnO nanoparticle with a diameter of 6-10 nm are uniformly dispersed in an ethanol solvent to form the solution with a concentration of 30 mg/ml. An about 200 nm thick zinc oxide (ZnO) layer was deposited on the cathode Au as the electron transporting layer (ETL) for the OPD. The BHJ active layer of about 850 nm thickness was made of an electron-donating semiconducting polymer poly (3-hexylthiophene) (P3HT) and an electron-accepting

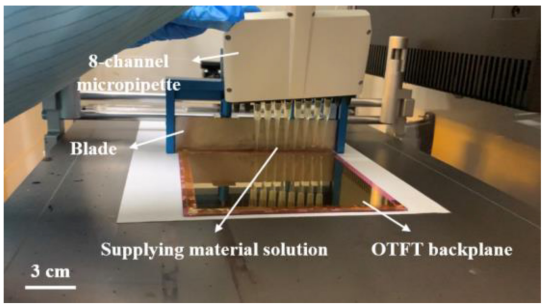

FIGURE 3. **Experimental setup of the doctor-blade coating process for large area coating of the active layer and the electron transporting layer (ETL) in the OPD using an 8-channel micropipette to supply the ink solution.**

fullerene derivative [6, 6]-phenyl-C61 butyric acid methyl ester (PCBM). The active layer solution (60 mg/ml) is prepared by mixing P3HT and PCBM (30:30 mg/ml) together, adding chlorobenzene (CB) and chloroform (CF) as solvents (volume ratio = 1:1) and then heating and stirring for more than 4 hours.

Both the ZnO and the BHJ layers were deposited by a facile doctor-blade coating process over large area with the experimental setup as shown in Fig. 3. An 8-channel micropipette was used to supply the material solutions for the coating processes. The moving speed of the blade was set to be 10 mm/s. The substrate was kept at the room temperature during all the processes. To obtain uniform film thickness over large area, the material solutions were coated twice along reverse directions. After coating, thermal annealing at 85 °C for 15 minutes in air was used to remove the solvent to form the solid films. All processes were carried out in the ambient lab environment with a controlled relative humility (RH < 20 %). An about 20 nm thick hole transporting layer (HTL) molybdenum oxide (MoO_x) was thermally evaporated on top. Finally, the top semi-transparent anode was deposited by thermal evaporation of silver (Ag) with an optimal thickness of about 9 nm. The maximum processing temperature for the OPD didn't exceed 100 °C so that the underneath OTFT part is not affected.

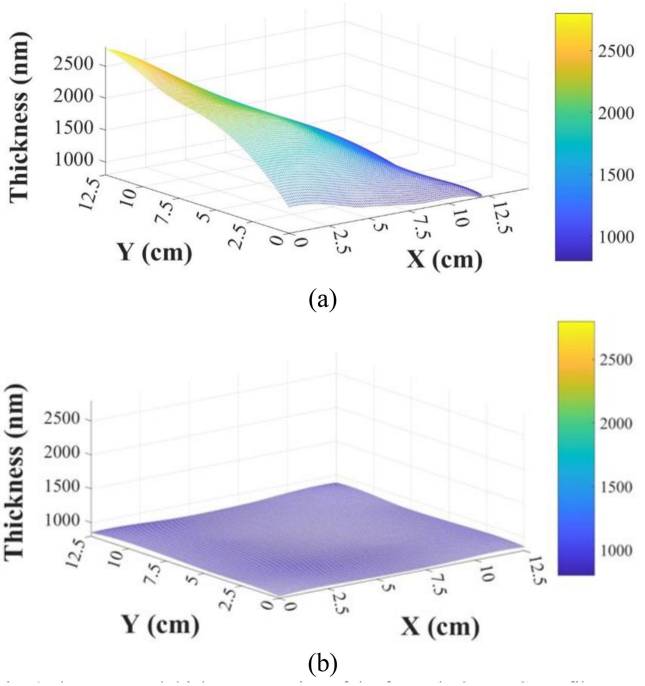

FIGURE 4. **The measured thickness mapping of the formed P3HT:PCBM films over a 12.5 cm × 12.5 cm area through different coating processes: (a) coating solution once and (b) coating solution twice along reverse directions.**

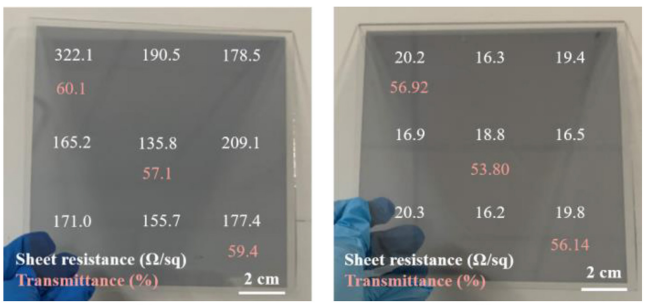

FIGURE 5. **Photo image of the fabricated MoO_x/Ag thin film on a 12.5 cm × 12.5 cm size glass substrate with the Ag deposition rate of (a) 0.7 Å/s and (b) 0.4 Å/s, showing the measured conductivity and transmittance over the area.**

III. RESULTS AND DISCUSSION

A. PROPERTIES OF FUNCTIONAL LAYERS

During the blade coating process, the dropped ink solution at the start location was brought to the whole area of the substrate by the blade. This caused thickness decrease of the formed P3HT: PCBM film along the coating direction, as shown in Fig. 4(a). By coating solution twice along the reverse directions, a P3HT: PCBM film of much improved uniformity was able to be achieved (Fig. 4(b)). Based on this approach, a uniform active layer of about 800 nm thickness was able to be obtained over large area (12.5 cm × 12.5 cm) for OPD integration. Since the OPD is on top of the OTFT in the active-matrix pixels, front-illumination is preferred to maximize the aperture ratio. Therefore, the top electrode needs to meet both requirements in conductivity and transmittance. It is shown in Fig. 5(a) and (b) that, at a slower evaporation rate (0.4 Å/s), the film of the same thickness (about 10 nm) is denser, and thus has higher conductivity at the similar transparency. After optimization, a semi-transparent conductive Ag film of uniform electrical and optical properties over large area (12.5 cm × 12.5 cm) was obtained (Fig. 5(b)). This sample is prepared by sequentially depositing MoO_x and the Ag thin film on a glass substrate, which could restore the path of the top incident light to the active layer more realistically. After addressing the large-area processing issues of these key functional layers, the OPD front-plane was able to be integrated onto the OTFT back-plane for large-area active-matrix imaging array.

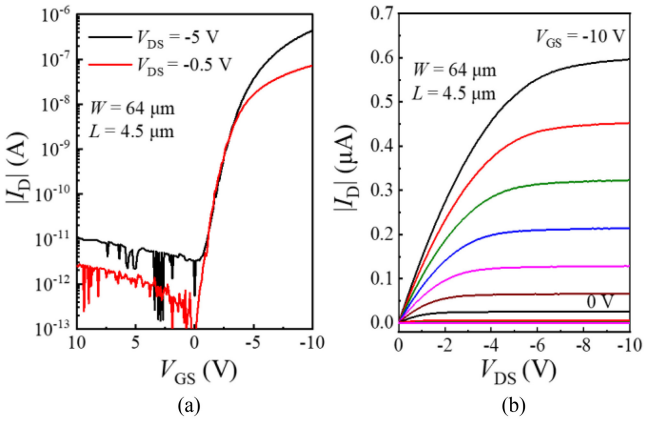

FIGURE 6. The measured typical electrical characteristics of the OTFT with the channel width and channel length of 64 μm and 4.5 μm, respectively. (a) transfer characteristic (I_D-V_{GS}) and (b) output characteristic (I_D-V_{DS}).

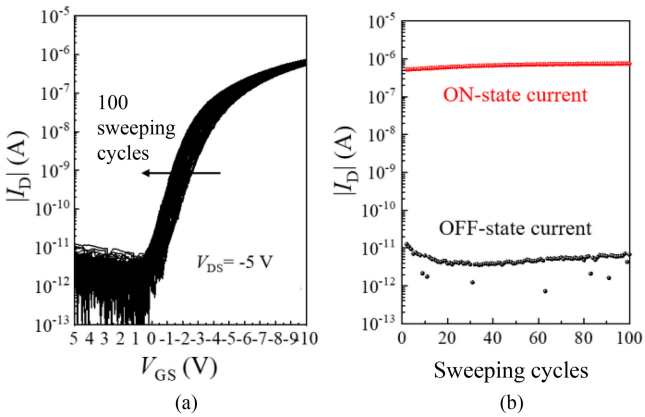

FIGURE 7. (a) The measured I_D-V_{GS} characteristics after multiple sweeping of V_{GS} between ON and OFF states for 100 cycles. (b) The extracted ON current and OFF current with the 100 sweeping cycles.

B. DEVICE PERFORMANCE

The measured typical transfer (I_D-V_{GS}) and output (I_D-V_{DS}) characteristics of the OTFT are given in Fig. 6, showing decent performance for pixel switching, including large ON/OFF ratio of 10^6 and negligible hysteresis. After multiple sweeping of V_{GS} between ON and OFF states for 100 cycles, the OTFT can maintain the ON/OFF ratio, indicating good enough stability for the pixel switches (Fig. 7).

The current-voltage characteristics of the fabricated OPD under dark condition and illumination with a green light (wavelength of 530 nm) at various power densities are given in Fig. 8. The dark current density is about 10^{-8} A/cm^2, and the responsivity is 0.1877 A/W at −6 V. Although the devices are processed in air ambient with relatively large area, the results are typical values for the reported P3HT: PCBM based OPDs [31], [45]. The OTFT performance before and after the OPD integration is shown in Fig. 8(c)), showing nearly no influence by the low-temperature solution processes of the OPD.

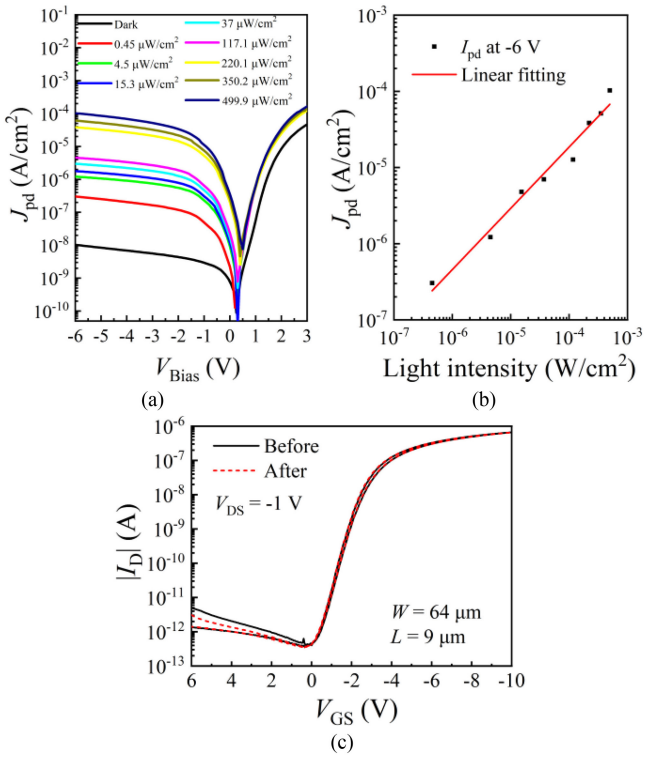

FIGURE 8. (a) The measured current-voltage characteristics of the fabricated OPD under dark condition and illumination with a green light (wavelength of 530 nm) at various power densities. (b) The measured current density as a function of the light power density and the fitting curve. The responsivity is calculated to be 0.1877 A/W at -6 V. (c) The measured electrical characteristic of the switch OTFT before (black solid line) and after (red dashed line) the OPD integration processes.

C. IMAGER SYSTEM

Based on the OTFT-OPD integration structure and processes, a flexible active-matrix imager was designed and fabricated. The designed imager has an effective imaging area of 130 mm × 130 mm with 1536 × 1536 pixels (about 300 ppi), and the pixel size is 85 μm × 85 μm (Fig. 9(a)). The gate and readout IC chips-on-flex were bonded on the peripheral pins of the imager array (Fig. 9(b)), and then connected to a FPGA based control system. Schematic of the readout circuitry is shown in Fig. 9 (c). In each pixel, the photo-generated charge is converted to a voltage output through a charge amplifier for further analog to digital conversion. The experimental setup for characterizing the imager system is shown in Fig. 10. The obtained imaging signals under ambient light were sent to a laptop computer for processing and displaying. Fig. 11 shows that the imagers can be used to clearly reproduce the different patterns, including the high-resolution fingerprint ones. The obtained images through the system in Fig. 11(a) and (b) used "OTFT" and "OPD" structures in paper and a printed fingerprint pattern on plastic film, respectively. For the later, the noisy background is due to light leakage through the printed black areas on the plastic film. The key figure-of-merits of the imager is compared to previously reported all-organic image sensor arrays in Table 1 [10], [37], [38]. It can

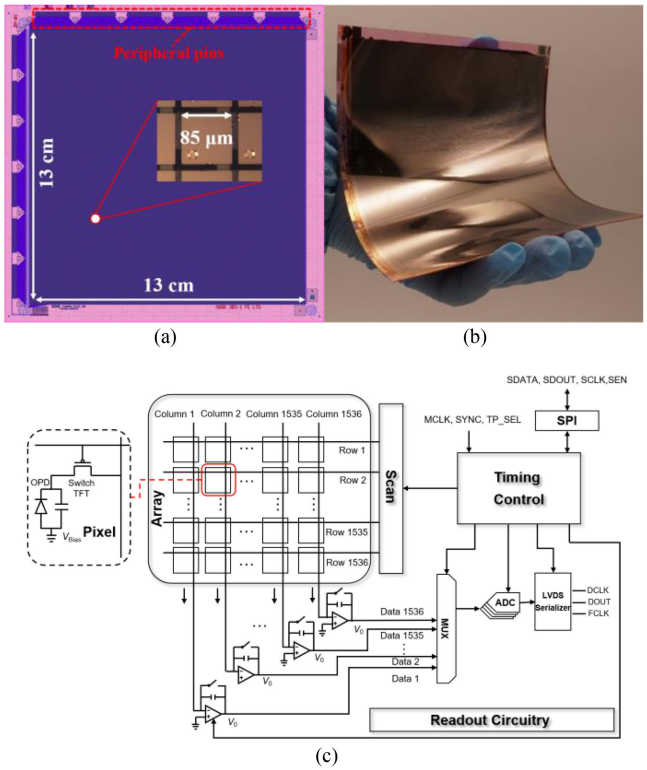

FIGURE 9. **(a) The layout design of the OTFT backplane, showing an effective area of 130 mm × 130 mm and a pixel size of 85 μm × 85 μm. (b) Photo image of the fabricated all-organic integrated flexible OPD-OTFT active-matrix imager. (c) Schematic of the imager array and the readout circuitry.**

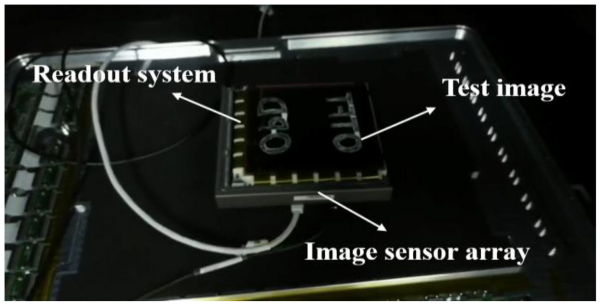

FIGURE 10. **Experimental setup for characterizing the fabricated imager.**

be concluded that this work achieves the largest area and highest resolution, but at the lowest process temperature (100 °C). The figure-of-merits is even better to the state-of-the-art OPD imagers using inorganic TFTs, which, however, require a process temperature higher than 300 °C [26], [38], [43].

IV. CONCLUSION

This work develops large-area low-temperature solution-based processes for fabricate flexible all-organic integrated active-matrix imagers. The demonstrated active-matrix imagers have the largest size and highest resolution among all reported OPD based imagers, but at the lowest process temperature. This work well proves the advantages

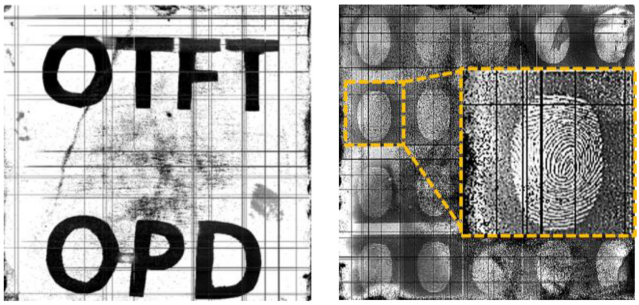

FIGURE 11. **The reproduced images through the fabricated all-organic integrated imagers using "OTFT" and "OPD" structures in paper and a printed fingerprint pattern on plastic film, respectively.**

TABLE 1. **Comparison of this work with all-organic image sensor arrays.**

Area (cm×cm)	Array Size	Resolution (ppi)	Maximum Process Temperature (°C)	Reference
5×5	72×72	36	180	[19]
1.5×1.5	32×32	54	150	[20]
3.6×3.6	12×13	8	120	[24]
13×13	1536×1536	300	100	This work

of organic semiconductor technologies and would provide a commercially competitive way for manufacturing high performance imagers in Internet-of-Everything applications. For some practical applications, such as the x-ray imager, radiation hardness of the used organic material stack needs to be further investigated.

REFERENCES

[1] K. Yoon, C. Kim, B. Lee, and D. Lee, "Single-chip CMOS image sensor for mobile applications," *IEEE J. Solid-State Circuits*, vol. 37, no. 12, pp. 1839–1845, Dec. 2002, doi: 10.1109/jssc.2002.804349.

[2] N. Akahane, S. Sugawa, S. Adachi, and K. Mizobuchi, "Wide dynamic range CMOS image sensors for high quality digital camera, security, automotive and medical applications," in *Proc. IEEE Sensors*, Oct. 2006, pp. 396–399, doi: 10.1109/ICSENS.2007.355489.

[3] E. R. Fossum, "CMOS image sensors: Electronic camera-on-a-chip," *IEEE Trans. Electron Devices*, vol. 44, no. 10, pp. 1689–1698, Oct. 1997, doi: 10.1109/16.628824.

[4] B. Pain *et al.*, "A low-power digital camera-on-a-chip implemented in CMOS active pixel approach," in *Proc. 12th Int. Conf. VLSI Design*, Goa, India, Jan. 1999, pp. 26–31, doi: 10.1109/ICVD.1999.745119.

[5] B. Goldstein *et al.*, "CMOS low current measurement system for biomedical applications," *IEEE Trans. Biomed. Circuits Syst.*, vol. 6, no. 2, pp. 111–119, Apr. 2012, doi: 10.1109/tbcas.2011.2182512.

[6] J. Ohta, T. Tokuda, K. Sasagawa, and T. Noda, "Implantable CMOS biomedical devices," *Sensors*, vol. 9, no. 11, pp. 9073–9093, Nov. 2009, doi: 10.3390/s91109073.

[7] T. Tokuda, A. Yamamoto, K. Kagawa, M. Nunoshita, and J. Ohta, "A CMOS image sensor with optical and potential dual imaging function for on-chip bioscientific applications," *Sens. Actuators A Phys.*, vol. 125, no. 2, pp. 273–280, Jan. 2006, doi: 10.1016/j.sna.2005.08.023.

[8] S. Fischer, N. Schibli, and F. Moscheni, "Design and development of the smart machine vision sensor (SMVS)," in *Proc. SPIE-Adv. Focal Plane Arrays Electron. Cameras II*, Zurich, Switzerland, Sep. 1998, pp. 186–192, doi: 10.1117/12.324011.

[9] H. Golnabi and A. Asadpour, "Design and application of industrial machine vision systems," *Robot. Comput. Integr. Manuf.*, vol. 23, no. 6, pp. 630–637, Dec. 2007, doi: 10.1016/j.rcim.2007.02.005.

[10] P. Egan, F. Lakestani, M. P. Whelan, and M. J. Connelly, "Three-dimensional machine vision utilising optical coherence tomography with a direct read-out CMOS camera," in *Proc. SPIE*, Munich, Germany, Jun. 2005, pp. 427–436, doi: 10.1117/12.612087.

[11] J. Oliveira, R. Brito-Pereira, B. F. Gonçalves, I. Etxebarria, and S. Lanceros-Mendez, "Recent developments on printed photodetectors for large area and flexible applications," *Org. Electron.*, vol. 66, pp. 216–226, Mar. 2019, doi: 10.1016/j.orgel.2018.12.028.
[12] F. Roy *et al.*, "Challenges in CMOS-based images," *Phys. Status Solidi C*, vol. 11, no. 1, pp. 50–56, Dec. 2013, doi: 10.1002/pssc.201300378.
[13] A. J. P. Theuwissen, "CMOS image sensors: State-of-the-art," *Solid State Electron.*, vol. 52, no. 9, pp. 1401–1406, 2008, doi: 10.1016/j.sse.2008.04.012.
[14] F. Arca, E. Kohlstädt, S. F. Tedde, P. Lugli, and O. Hayden, "Large active area organic photodiodes for short-pulse X-ray detection," *IEEE Trans. Electron Devices*, vol. 60, no. 5, pp. 1663–1667, May 2013, doi: 10.1109/ted.2013.2250974.
[15] K. S. Budil *et al.*, "The flexible X-ray imager," *Rev. Sci. Instrum.*, vol. 67, no. 2, pp. 485–488, 1998, doi: 10.1063/1.1146616.
[16] G. H. Gelinck *et al.*, "X-ray imager using solution processed organic transistor arrays and bulk heterojunction photodiodes on thin, flexible plastic substrate," *Org. Electron.*, vol. 14, no. 10, pp. 2602–2609, Jul. 2013, doi: 10.1016/j.orgel.2013.06.020.
[17] M. Hoheisel, "Review of medical imaging with emphasis on X-ray detectors," *Nucl. Instrum. Methods Phys. Res. A, Accelerators Spectrometers Detect. Assoc. Equip.*, vol. 563, no. 1, pp. 215–224, 2006, doi: 10.1016/j.nima.2006.01.123.
[18] D. Tordera *et al.*, "A high-resolution thin-film fingerprint sensor using a printed organic photodetector," *Adv. Mater. Technol.*, vol. 4, no. 11, 2019, Art. no. 1900651, doi: 10.1002/admt.201900651.
[19] T. Kamada *et al.*, "OLED display incorporating organic photodiodes for fingerprint imaging," *J. Soc. Inf. Display*, vol. 27, no. 6, pp. 361–371, 2019, doi: 10.1002/jsid.786.
[20] J. H. Koo, D. C. Kim, H. J. Shim, T.-H. Kim, and D.-H. Kim, "Flexible and stretchable smart display: Materials, fabrication, device design, and system integration," *Adv. Funct. Mater.*, vol. 28, no. 35, 2018, Art. no. 1801834, doi: 10.1002/adfm.201801834.
[21] A. Nathan and S. Gao, "Interactive displays: The next omnipresent technology," *Proc. IEEE*, vol. 104, no. 8, pp. 1503–1507, Aug. 2016, doi: 10.1109/jproc.2016.2582578.
[22] Q. Lu *et al.*, "Bio-inspired flexible artificial synapses for pain perception and nerve injuries," *NPJ Flexible Electron.*, vol. 4, no. 1, pp. 1–8, Mar. 2020, doi: 10.1038/s41528-020-0066-0.
[23] Y. Wang, Y. Yu, J. Guo, Z. Zhang, X. Zhang, and Y. Zhao, "Bio-inspired stretchable, adhesive, and conductive structural color film for visually flexible electronics," *Adv. Funct. Mater.*, vol. 30, no. 32, 2020, Art. no. 2000151, doi: 10.1002/adfm.202000151.
[24] H. Akkerman *et al.*, "Large-area optical fingerprint sensors for next generation," in *SID Symp. Dig. Tech. Papers*, May 2019, pp. 1000–1003, doi: 10.1002/sdtp.13095.
[25] T. Kaneko, Y. Hosokawa, M. Tadauchi, Y. Kita, and H. Andoh, "400 dpi integrated contact type linear image sensors with poly-Si TFT's analog readout circuits and dynamic shift registers," *IEEE Trans. Electron Devices*, vol. 38, no. 5, pp. 1086–1093, May 1991, doi: 10.1109/16.78383.
[26] T. N. Ng, R. A. Lujan, S. Sambandan, R. A. Street, S. Limb, and W. S. Wong, "Low temperature a-Si: H photodiodes and flexible image sensor arrays patterned by digital lithography," *Appl. Phys. Lett.*, vol. 91, no. 6, 2007, Art. no. 063505, doi: 10.1063/1.2767981.
[27] J. Kim *et al.*, "A study on H2 plasma treatment effect on a-IGZO thin film transistor," *J. Mater. Res.*, vol. 27, no. 17, pp. 2318–2325, 2012, doi: 10.1557/jmr.2012.199.
[28] T. Toda, D. Wang, J. Jiang, M. P. Hung, and M. Furuta, "Quantitative analysis of the effect of hydrogen diffusion from silicon oxide etch-stopper layer into amorphous In–Ga–Zn–O on thin-film transistor," *IEEE Trans. Electron Devices*, vol. 61, no. 11, pp. 3762–3767, Nov. 2014, doi: 10.1109/TED.2014.2359739.
[29] S. M. Menke, R. Pandey, and R. J. Holmes, "Tandem organic photodetectors with tunable, broadband response," *Appl. Phys. Lett.*, vol. 101, no. 22, 2012, Art. no. 223301, doi: 10.1063/1.4768807.
[30] S. Xing, X. Wang, E. Guo, H. Kleemann, and K. Leo, "Organic thin-film red-light photodiodes with tunable spectral response via selective exciton activation," *ACS Appl. Mater. Interfaces*, vol. 12, no. 11, pp. 13061–13067, Mar. 2020, doi: 10.1021/acsami.9b22058.
[31] T. N. Ng, W. S. Wong, M. L. Chabinyc, S. Sambandan, and R. A. Street, "Flexible image sensor array with bulk heterojunction organic photodiode," *Appl. PhyS. Lett.*, vol. 92, no. 21, May 2008, Art. no. 213303, doi: 10.1063/1.2937018.
[32] G. H. Gelinck *et al.*, "X-ray detector-on-plastic with high sensitivity using low cost, solution-processed organic photodiodes," *IEEE Trans. Electron Devices*, vol. 63, no. 1, pp. 197–204, Jan. 2016, doi: 10.1109/ted.2015.2432572.
[33] T. Yokota *et al.*, "A conformable imager for biometric authentication and vital sign measurement," *Nat. Electron.*, vol. 3, no. 2, pp. 113–121, Feb. 2020, doi: 10.1038/s41928-019-0354-7.
[34] X. Guo *et al.*, "Current status and opportunities of organic thin-film transistor technologies," *IEEE Trans. Electron Devices*, vol. 64, no. 5, pp. 1906–1921, May 2017, doi: 10.1109/TED.2017.2677086.
[35] K. C. Dickey, J. E. Anthony, and Y.-L. Loo, "Improving organic thin-film transistor performance through solvent-vapor annealing of solution-processable triethylsilylethynyl anthradithiophene," *Adv. Mater.*, vol. 18, no. 13, pp. 1721–1726, Jun. 2006, doi: 10.1002/adma.200600188.
[36] M. Banach, S. Markham, R. Agaiby, and P. Too, "Low leakage organic backplanes for high pixel density optical sensors," in *SID Symp. Dig. Tech. Papers*, May 2018, pp. 90–91, doi: 10.1002/sdtp.12566.
[37] A. Kumar *et al.*, "X-ray imaging sensor arrays on foil using solution processed organic photodiodes and organic transistors," in *Proc. SPIE*, Brussels, Belgium, May 2014, Art. no. 91370Q, doi: 10.1117/12.2051224.
[38] T. Someya *et al.*, "Integration of organic FETs with organic photodiodes for a large area, flexible, and lightweight sheet image scanners," *IEEE Trans. Electron Devices*, vol. 52, no. 11, pp. 2502–2511, Nov. 2005, doi: 10.1109/ted.2005.857935.
[39] H. Wang, H. Liu, Q. Zhao, C. Cheng, W. Hu, and Y. Liu, "Three-component integrated ultrathin organic photosensors for plastic optoelectronics," *Adv. Mater.*, vol. 28, no. 4, pp. 624–630, Jan. 2016, doi: 10.1002/adma.201503953.
[40] T. Agostinelli, B. Yaglioglu, I. Horne, and S. Markham, "Low leakage organic backplanes for low power and high pixel density flexible displays," in *SID Symp. Dig. Tech. Papers*, May 2016, pp. 1523–1525.
[41] H. Kim, Y. Bonnassieux, and G. Horowitz, "Fundamental benefits of the staggered geometry for organic field-effect transistors," *IEEE Electron Device Lett.*, vol. 32, no. 9, pp. 1302–1304, Sep. 2011, doi: 10.1109/LED.2011.2160249.
[42] L. Han, Y. Huang, W. Tang, S. Chen, J. Zhao, and X. Guo, "Reducing contact resistance in bottom contact organic field effect transistors for integrated electronics," *J. Phys. D Appl. Phys.*, vol. 53, no. 1, Oct. 2019, Art. no. 014002, doi: 10.1088/1361-6463/ab42a9.
[43] C. Liu, Y. Xu, and Y. Y. Noh, "Contact engineering in organic field-effect transistors," *Mater. Today*, vol. 18, no. 2, pp. 79–96, Mar. 2015, doi: 10.1016/j.mattod.2014.08.037.
[44] M. J. Harding, I. P. Horne, and B. Yaglioglu, "Flexible LCDs enabled by OTFT," in *SID Symp. Dig. Tech. Papers*, Los Angeles, CA, USA, Jun. 2017, pp. 793–796, doi: 10.1002/sdtp.11754.
[45] K. Y. Kim *et al.*, "Flexible narrowband organic photodiode with high selectivity in color detection," *Nanotechnology*, vol. 30, no. 43, Oct. 2019, Art. no. 435203, doi: 10.1088/1361-6528/ab35ff.